///VSP///
Advanced Robotics 22 (2008) 119–140
ADVANCED ROBOTICS
www.brill.nl/ar

Full paper

Probing Virtual Boundaries and the Perception of Delayed Stiffness

Assaf Pressman [a,b], **Ilana Nisky** [b], **Amir Karniel** [b] **and Ferdinando A. Mussa-Ivaldi** [a,*]

[a] Sensory Motor Performance Program, Rehabilitation Institute of Chicago, 345 E. Superior Street, Chicago, IL 60611-2654, USA

[b] Department of Biomedical Engineering, Ben-Gurion University of the Negev, Beer-Sheva 84105, Israel

Received 7 November 2006; accepted 28 May 2007

Abstract

During interaction with robotic manipulanda, the human brain constructs internal representations of the environment imposed by the robotic device. These representations (i) provide cognitive interpretation of the interfaced environment and (ii) generate motor commands for future interaction with the imposed environment. Interestingly, cognitive and motor representations are not always mutually consistent. We consider a simple environment consisting of a spring-like surface, where either the delay between force and position or the location of the boundary is experimentally altered. We explored the cognitive representation of rigidity by asking subjects which of two surfaces is stiffer. We also considered the motor representation by investigating adaptation to the same virtual environments. We asked subject to reach a target inside virtual surface, and observed adaptation and its after effects in catch trials. In the cognitive study, we constructed psychometric curves based on the verbal reports of the subjects. In the motor study, we constructed analogous curves, which we name 'motormetric curves', describing the implicit motor expectation of rigidity, as expressed not verbally but by the errors in catch trials, where the delay was unexpectedly removed. We simulated motormetric curves from a simplified mechanical model of the arm and neural controller. We found that the cognitive reports reflected our measure of the motor behavior in the case of delayed stiffness, but not in the case of shifted boundary.

Keywords

Stiffness, robotic manipulandum, telemanipulation, perception, human–machine interface

1. Introduction

At the heart of neuroscience lies a search for understanding how the environment affects the nervous system and how the nervous system, in turn, alters the envi-

* To whom correspondence should be addressed. E-mail: sandro@northwestern.edu

 DOI:10.1163/156855308X291863

ronment [1]. Robotic devices, as interactive tools, when properly combined with computational models can lead to a deeper understanding of the nervous system, in general, and of the motor control system, in particular.

A prominent line of research employs robotic manipulanda to generate force perturbations during reaching movements, with the goal of revealing how the brain adapts to novel dynamics [2–8]. This methodology has recently yielded clinical applications for diagnosis and rehabilitation [9–11]. It is important to note that adaptation to force perturbations is a form of procedural learning, occurring implicitly without full awareness on the part of the learning subject [12].

Another promising research direction employs robotic devices to generate virtual reality and explore the haptic experience of virtual or remote objects [13–17]. In contrast to the implicit nature of adaptation to force perturbations these studies usually involve explicit knowledge of the task and the subjects are occasionally asked to report their haptically induced perception.

In this study we consider both the explicit cognitive representation of the environment and the implicit representation associated with adaptation to delayed and shifted surfaces.

The use of delayed forces in our experiments is consistent with a common circumstance of bidirectional telemanipulation. There, the human operator controls a master robotic manipulandum and receives delayed force feedback from a remote physical object being manipulated by a remote slave robot [18–21]. Under these conditions, the design of effective interfaces requires some understanding of the neural processes underlying perception and control in the presence of delays. Thus, it was suggested that the brain may employ computations analogous to a Smith Predictor [22, 23] or Wave Variables [24] for compensating for the effects of delays. The ability of the nervous system to adaptively control reaching movements under various external force perturbations has been investigated for state-dependent forces [3, 25, 26] and for time-dependent forces [5, 27]; however, the ability to perceive, represent and adapt to delayed force perturbations has not yet been systematically explored. In particular, the influence of delays on the perceived mechanical properties of a remote object was largely overlooked.

In a recent study we found a consistent influence of the delay between force and position on the perception of stiffness [28]. When subjects were asked to judge between two surfaces, where in one of the two the force applied by the manipulator was either temporally leading or lagging the position imposed by the subject, they consistently reported the surface in which the force lagged position as stiffer and the other as more compliant.

To further explore this recent result, we have simulated an arm model and developed an adaptation paradigm and a new measure of the implicit expectation, which we call the ‘motormetric curve’. Our main objective was to use this tool to compare verbal and motor responses to contact with delayed and shifted surfaces (which will be defined later in Section 2.1). Interestingly, as described below, the explicit reply of the subjects measured by the psychometric curves did not always match the implicit expectations as measured by the motormetric curves.

In Section 2, we describe our method for using robotic manipulandum to study the behavioral and perceptual aspects of stiffness and boundary perception. In Section 3, we present a simple model for the arm and neural controller, and the prediction of the expected behavior in probing before and after adaptation. The behavioral results are presented in Section 4. Finally, we discuss the results and the possible implications and applications of this research methodology in Section 5.

2. Methods

We employed a planar 2-d.o.f. robotic manipulandum to generate spring-like surfaces (SLS) which were used to determine the implicit and explicit behavior of the subjects. Two types of SLS where rendered: one in which the force was lagging the position (delayed SLS, see equation (1)) and another in which the SLS was shifted (shifted SLS). Subjects interacted with these surfaces in an attempt to determine their stiffness.

In a recent study we used a forced choice paradigm, where subjects probed two surfaces and had to answer which surface felt stiffer. We found clear overestimation of delayed stiffness [28]. In an attempt to limit cognitive influences on the results we developed a new protocol and an objective measure of the expected stiffness based on the hand movement at catch trials, where delays were unexpectedly removed.

We designed the experiments based on the following assumptions:

(i) Subjects can rapidly learn to perform an accurate back and forth ‘slicing’ movement with the peak penetration at a predefined goal as they probe a virtual surface.

(ii) Subjects plan their movements based on the expected stiffness, estimated according to the preceding probing movements.

(iii) The control of the rapid slicing movement is a feed-forward control. The effect of feedback during the movement is neglected, and sensory information is used only to estimate the stiffness and to modify the motor command of the next movement.

Provided the assumptions above, subjects who are trained to perform slicing movement to a certain point inside the surface are expected to miss the target (overshoot/undershoot) whenever the surface properties are unexpectedly changed. The amount of overshoot/undershoot is expected to be a monotonic function of the gap between the estimated and effective stiffness. Consider the following example: a subject is trained in a delayed SLS and then experiences a non-delayed SLS with the same level of stiffness. This unexpected removal of a perturbation in a learning paradigm is called a ‘catch trial’. If the delayed stiffness is overestimated we expect to observe an overshoot in a catch trial. We first describe the experimental protocols and then the data analysis used to construct the motormetric curves based on these assumptions.

2.1. Subjects, Apparatus and Experimental Protocols

Thirteen subjects participated in the experiments after signing the informed consent form approved by Northwestern's Institutional Review Board. Seated subjects held with their right hand the handle of a 2-d.o.f. robotic manipulandum and looked at a screen, placed horizontally above their hand, which displayed a virtual SLS as colored wide squares (Figs 1 and 2). For further details about the robotic manipulandum, see Refs [4, 31]. The robotic manipulandum exerted forces on the subject's hand and acquired its trajectory. The location of the hand was displayed by a line

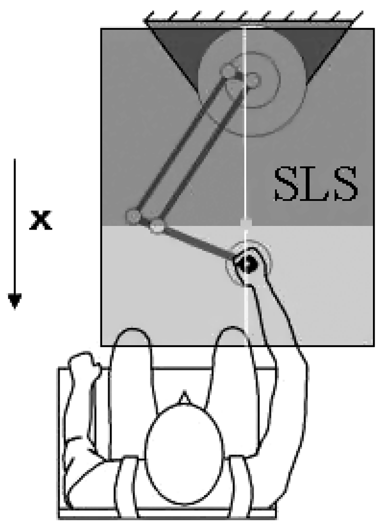

Figure 1. The SLS. A subject holding the robotic manipulandum probing a SLS with or without delay. During the experiment, the robotic manipulandum, as well as the position of the subject's hand were not visible to the subject, who saw only the projected SLS and a vertical line indicating the location of his hand along the y-axis. A bright point was projected at a fixed location and the subject was instructed to keep the line near this point. With a delayed SLS the subject experienced forces proportional to the position reached τ seconds before, i.e., $F_x(t) = -K(X(t-\tau) - X_0)$.

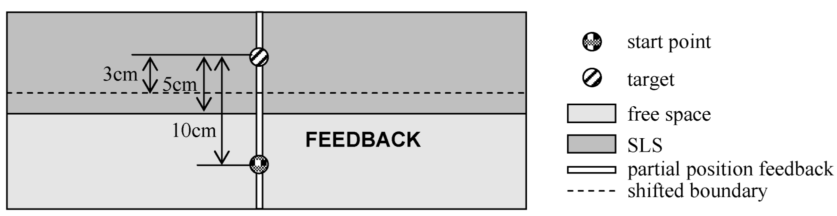

Figure 2. Schematic view of the experimental screen. Subjects were instructed to move their hand (that holds the manipulandum) from the start point to the target and back, very fast, while maintaining the white line location as constant as possible.

perpendicular to the boundary of the object. This provided subjects with partial position information, which included the lateral position of the hand without revealing the degree of penetration inside the virtual object. By keeping this line at the same location, subjects contacted the objects at a fixed configuration of the arm.

Two types of data were acquired:

(i) The position of the hand along the x-axis, sampled at a rate of 100 samples per second.

(ii) The interaction force with the surface. This force was calculated in real-time based on the hand position, the delay and the elastic properties of the surface (stiffness and boundary).

The force exerted by the virtual surfaces was in the x-axis direction (see Fig. 1), in proportion to the displacement from the boundary, X_0:

$$F_x(t) = \begin{cases} -K(X(t-\Delta t) - X_0) & X(t-\Delta t) > X_0 \\ 0 & X(t-\Delta t) \leqslant X_0, \end{cases} \tag{1}$$

where $F_x(t)$ is the force in the x-axis direction, K is the spring's stiffness constant, $X(t)$ is the position along the x-axis, X_0 is the coordinate of the boundary, and Δt is the delay between force exerted on the hand and its position.

2.1.1. Experiment 1: Motormetric for Delayed Surface

Six subjects participated in this experiment (three males and three females). Two circles were projected on the SLS (Fig. 2). One, the target, was 5 cm beyond the non-shifted surface boundary (X_0 in (1)). The second, the start point, was located 5 cm away from the boundary, in the direction of the subject. Subjects were instructed to reach the target and then return to the start point. Such a slicing movement completed a single trial. Performance feedback was provided as colored written text messages (red 'long', yellow 'short' and blue 'right').

The experiment (a total of 1301 trials), consisted of four phases (see Table 1 for a detailed description):

(i) Null field training — 30 slicing movements in free space allowing subjects to become acquainted with the manipulandum dynamics and the slicing task.

(ii) Null delay training — 50 slicing movements with 10 randomly ordered blocks of SLS with stiffness levels chosen from the group {150 to 600 in jumps of 50 N/m}, five trials in each block, allowing subjects to become acquainted with the various stiffness levels that will be presented during the experiment.

(iii) Delay training — 20 slicing movements with constant stiffness level SLS ($K =$ 375 N/m), where the force feedback lagged the position by 50 ms.

(iv) Test — 1201 slicing movements. The subject was introduced to a surface (D-surface) with a stiffness level of $K_{\text{trained}} = 375$ N/m and Δt either 0 or 50 ms (see (1)) for a number of consecutive trials (four to six, randomly chosen). Following this series a catch trial was introduced, where Δt was set to

Table 1.
Delayed motormetric experiment phases

Phase	K (N/m)	Δt (ms)	Feedback	Number of trials
Null field training	0	0	always	20
Null delay training	varying in randomly ordered blocks each stiffness appears 5 times	0	always	50
Delay training	375	50	always	30
Test	375 (with 16% catch trials of varying stiffness, at least four movements between catch trials)	42% 50; 42% 0; 16% catch 0	68%, never on catch trials and randomly not on training trials	1201 (200 of them catch trials)

zero (K-surface) and the stiffness level K_{catch} was altered to a random value chosen from the group {150 to 600 in jumps of 50 N/m}. During these catch trials and in one randomly selected trial in each training block, the feedback text message regarding the amount of penetration was not provided.

2.1.2. Experiment 2: Motormetric for Shifted Surface

Four subjects participated in this experiment (two males and two females; three of them participated in the previous experiment as well). This paradigm was almost identical to the delayed surface paradigm, but the delayed surfaces were replaced with boundaries shifted 2 cm away from the subject (into the surface, see dashed line in Fig. 2). In these cases the distance of the target from the boundary became 3 cm.

The choice of 50 ms as the delay between the position and the force feedback during surface interaction is motivated, as in our previous study [28], by the total duration of the slicing movement (about 400 ms). We have noticed that a long delay occupying a significant portion of the movement leads to abolishing the perception of a surface. When moving at typical velocity of 0.5 m/s, a delay of 50 ms causes an average boundary shift of 2 cm, motivating our selection of boundary shift. The choice of stiffness level exerted by the manipulandum was motivated by the actual plant of the machine and the maximum feasible exerted force, for the motion with an extent of several centimeters. The value of 375 N/m was the mid-range of the chosen stiffness levels of 150–600 N/m; therefore, the stiffness level of both compared SLS is never actually equal.

2.1.3. Experiment 3: Perception of Boundary Shift

Six subjects participated in this experiment (three for positive shift, three for negative shift). The experiment was based on a forced choice paradigm, where in each trial the subject was presented with two surfaces: one in which the stiffness was varied across trials (K-surface) and the other in which the zero position (i.e., the boundary location) of the surface varied across trials (D-surface). In the remainder of the paper D-surface or D-stiffness will indicate either 'displaced' (i.e., shifted) stiffness or 'delayed' stiffness according to the context, i.e., the experiment reported.

The two surfaces were represented by rectangles of different colors (red and green). The two colors were, however, assigned randomly, so that each surface type (K or D) was not uniquely associated with a color. Whenever the hand of the subject moved out of a surface by more than 10 cm, the objects switched between K and D types, and the display changed color accordingly. Subjects could switch between the two surfaces as many times as they pleased until they felt ready to answer the question: 'Which surface is stiffer (green or red)?'. The answer was given by the subject pressing one of two buttons on a custom-made hand-held device. No feedback was provided after each trial.

During each one of the 500 trials presented to the subject, the K-surface took one of the stiffness values drawn randomly from 150 to 600 N/m (in increments of 50 N/m). The stiffness of the D-surface was set to 375 N/m; therefore, the stiffness of K and D was never equal. The D-surface was shifted towards and away from the subject in random trials. The shift was implemented by changing the value of X_0 in (1). Values for X_0 were drawn from a Gaussian distribution ($\mu = \pm 1.5$ cm, $\sigma = 0.35$ cm). Each subject encountered either a positive or a negative shift (the sign of μ). The shift of the K-surface was set to X_0.

The experiment consisted of two blocks. The first was a reference block in which no shift of the boundary took place and lasted for 100 trials. In the second block (400 trials), on random trials spaced two to six trials apart, the boundary was shifted toward or away from the subject (for each subject, the direction of shift was fixed during the whole experiment). The response of the subject was recorded for each trial.

2.2. Data Analysis: Psychometric and Motormetric Curves

2.2.1. Psychometric Curves

The psychometric curve quantifies the subject's performance in a discrimination task. The psychometric function relates the subject's responses to an independent variable, usually some physical measure of the stimulus [29, 30]. Once the psychometric curve is fitted one can derive a threshold value of stimulus intensity for some desired performance level, using the inverse of the fitted psychometric function.

The general form of a psychometric function is:

$$\psi(x, \alpha, \beta, \gamma, \lambda) = \gamma + (1 - \gamma - \lambda) F(x, \alpha, \beta), \tag{2}$$

where x is the stimulus intensity. The shape of the curve is determined by the parameters $[\alpha, \beta, \lambda, \gamma]$ and the choice of a two-parameter function F, typically a sigmoid function. The 95% confidence intervals for estimated parameters are calculated using bootstrap [29, 30].

We derived the psychometric function by estimating the subject's probability to answer that the D-surface is stiffer than the K-surface as a function of the actual difference $\Delta K = K_\mathrm{D} - K_\mathrm{K}$.

This probability was calculated from the subject's answers according to:

$$P(\Delta K) = \frac{\sum_{n=1}^{N(\Delta K)} A[n]}{N(\Delta K)} \tag{3}$$

$$A[n] = \begin{cases} 1 & \text{D stiffer} \\ 0 & \text{K stiffer,} \end{cases} \tag{4}$$

where $A[n]$ is a binary representation of the subject's answer and $N(\Delta K)$ is the total number of trials with the given difference ΔK.

After fitting the psychometric curve we derived the 50% threshold value, the point of subjective equality (PSE), corresponding to the difference between the surfaces that is perceived to be zero.

A positive PSE value means underestimation of the D-stiffness, while a negative PSE value means overestimation of the D-stiffness (see Fig. 3).

2.2.2. Motormetric Curves

Similar to the psychometric curve, the motormetric curve relates the subject's performance to an independent variable. However, whereas the psychometric curves quantify verbal responses, the motormetric curves quantify motor responses.

We analyzed the difference between the estimated and actual stiffness by measuring the reaching errors (overshoot/undershoot) during catch trials. Therefore, the motormetric curve is essentially the overshoot probability. The motormetric curve is derived in a similar manner to the psychometric curve, but it describes the probability to overshoot in the catch trials as a function of the difference $K_\mathrm{trained} - K_\mathrm{catch}$. The 50% threshold in this function denotes the point of motor response equality (PMRE), in which the subject had equal probability to overshoot and to undershoot. The overshoot probability was calculated as follows:

$$P(\Delta K) = \frac{\sum_{n=1}^{N(\Delta K)} O[n]}{N(\Delta K)}, \quad n = \text{all catch trials with stiffness difference } \Delta K, \tag{5}$$

where $N(\Delta K)$ is the total number of catch trials in which the stiffness difference was ΔK:

$$O[n] = \begin{cases} 1 & p^\mathrm{c}[n] > p^\mathrm{t}[n] \\ 0 & \text{else,} \end{cases} \tag{6}$$

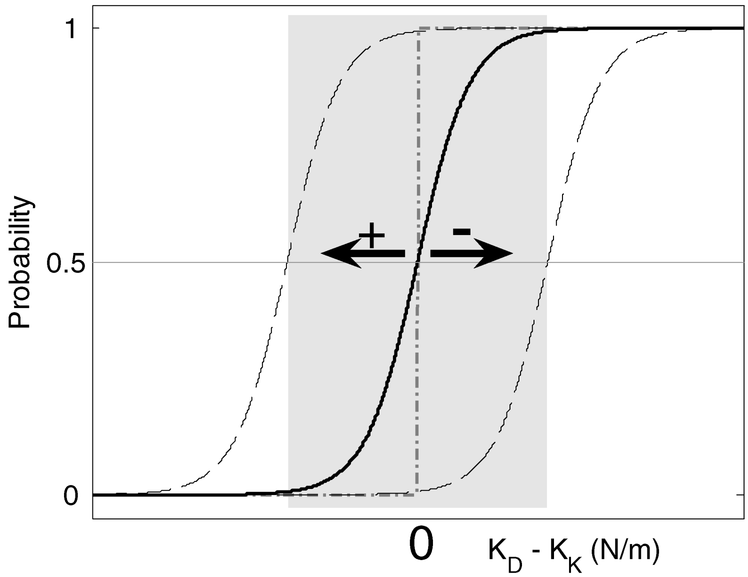

Figure 3. Possible psychometric curves for the expectation of an answer indicating that D is stiffer than K as a function of the difference in stiffness between surface D and K. The gray dot-dashed line demonstrates the performance of a 'perfect subject' who can accurately estimate whether surface D is stiffer than K. The black solid line shows a typical subject, who would make some mistakes in the transition region (marked as a gray rectangle). A shift in this graph to the left (right), as seen by the dashed black line on the left (right), would suggest the subject perceives surface D as stiffer (softer) than it really is.

is a binary representation of overshoot/undershoot, where $p^{c}[n]$ is the penetration measured at catch trial n and $p^{t}[n]$ is the median of the penetrations measured at the last three training trials preceding the nth catch trial.

Two penetration definitions were considered (Fig. 4):

- Absolute penetration $p_{a}[n]$: the penetration from the fixed coordinates origin.
- Relative penetration $p_{r}[n]$: the penetration from the force initiation point.

3. Biomechanical Model and Simulations

3.1. Model

In order to test the hypothesis that a simplified model can predict the same results as the subject, we simulated the arm as a two-link model. In this formulation we use mathematical models to formulate a hypothesis about how the central nervous system works. The human arm was modeled as a planar two-link manipulator, depicted in Fig. 5. The modeling assumes the mass and therefore dynamic of the robotic manipulandum can be neglected in comparison to a human's arm, and therefore the simulation concerns only the arm.

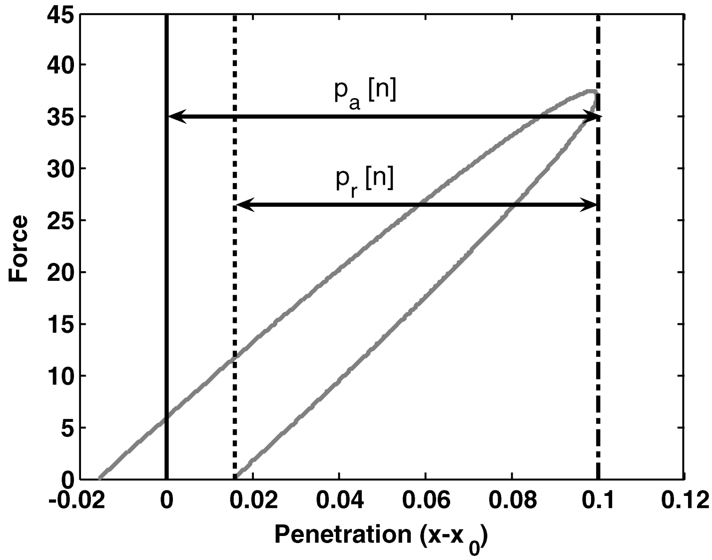

Figure 4. Absolute *versus* relative penetration. Absolute penetration $p_{\mathrm{a}}[n]$: the penetration from the fixed coordinates origin. Relative penetration $p_{\mathrm{r}}[n]$: the penetration from the force initiation point.

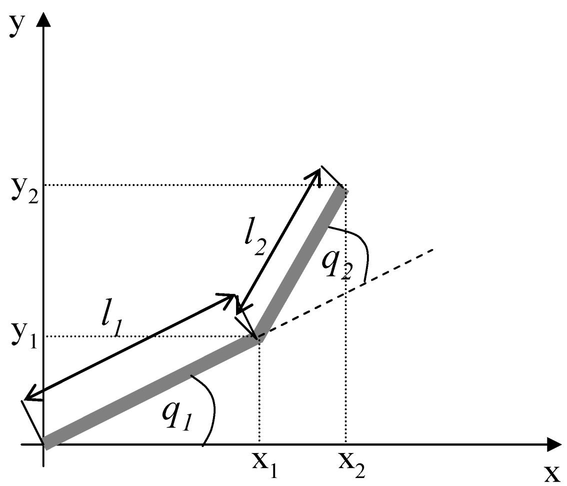

Figure 5. Planar two-link model for a human hand: l_i and q_i are the shoulder and forearm length and angle, respectively, and (x_i, y_i) are the Cartesian coordinates of the elbow and end-point.

Thus, the direct kinematics is:

$$\begin{pmatrix} x_1 \\ y_1 \end{pmatrix} = \begin{pmatrix} l_1 \cos(q_1) \\ l_1 \sin(q_1) \end{pmatrix}; \quad \begin{pmatrix} x_2 \\ y_2 \end{pmatrix} = \begin{pmatrix} x_1 \\ y_1 \end{pmatrix} + \begin{pmatrix} l_2 \cos(q_1 + q_2) \\ l_2 \sin(q_1 + q_2) \end{pmatrix} \tag{7}$$

$$\begin{pmatrix} \dot{x}_1 \\ \dot{y}_1 \end{pmatrix} = \mathbf{J}_1 \begin{pmatrix} \dot{q}_1 \\ \dot{q}_2 \end{pmatrix} = \mathbf{J}_1 \dot{\mathbf{q}}; \quad \begin{pmatrix} \dot{x}_2 \\ \dot{y}_2 \end{pmatrix} = \mathbf{J}_2 \dot{\mathbf{q}}, \tag{8}$$

where $l_{1,2}$ are the upper arm and forearm lengths respectively, $q_{1,2}$ are the shoulder and elbow joints angles, respectively, and:

$$\mathbf{J}_1 = \begin{pmatrix} -l_1 \sin(q_1) & 0 \\ l_1 \cos(q_1) & 0 \end{pmatrix} \tag{9}$$

$$\mathbf{J}_2 = \begin{pmatrix} -l_1 \sin q_1 - l_2 \sin(q_1 + q_2) & -l_2 \sin(q_1 + q_2) \\ l_1 \cos q_1 + l_2 \cos(q_1 + q_2) & l_2 \cos(q_1 + q_2) \end{pmatrix}, \tag{10}$$

are the elbow and end-point Jacobian matrices, respectively.

In generalized coordinates one can write the arm dynamics equations as:

$$\mathbf{H}(\mathbf{q})\ddot{\mathbf{q}} + \mathbf{C}(\mathbf{q}, \dot{\mathbf{q}})\dot{\mathbf{q}} + \mathbf{G} = \mathbf{Q}(\mathbf{q}, \dot{\mathbf{q}}, \mathbf{q}_{\mathrm{d}}(t)), \tag{11}$$

where $\mathbf{Q}(\mathbf{q}, \dot{\mathbf{q}}, \mathbf{q}_{\mathrm{d}}(t))$ are the joint torques generated by the controller as a function of the joints angles and desired joints trajectories $\mathbf{q}_{\mathrm{d}}(t)$:

$$\mathbf{H}(\mathbf{q}) = \begin{pmatrix} I_1 + I_2 + m_1 l_{c1}^2 + m_2(l_1^2 + l_{c2}^2 + 2 l_1 l_{c2} \cos(q_2)) & I_2 + m_2(l_{c2}^2 + l_1 l_{c2} \cos(q_2)) \\ I_2 + m_2(l_{c2}^2 + l_1 l_{c2} \cos(q_2)) & I_2 + m_2 l_{c2}^2 \end{pmatrix}, \tag{12}$$

is the inertial matrix, where $m_{1,2}$, $I_{1,2}$ and $l_{c1,2}$ are the upper arm and forearm mass, inertia and center of mass, respectively,

$$\mathbf{C}(\mathbf{q}, \dot{\mathbf{q}}) = \begin{pmatrix} -m_2 l_1 l_{c2} \sin(q_2)\dot{q}_2 & -m_2 l_1 l_{c2} \sin(q_2)(\dot{q}_1 + \dot{q}_2) \\ m_2 l_1 l_{c2} \sin(q_2)\dot{q}_2 & 0 \end{pmatrix}, \tag{13}$$

is the Coriolis and centripetal coefficients matrix and **G** is the gravitation forces which are zero in our planar horizontal simplified model. In the description of the controller, we represent the desired motions as explicit functions of time — analogous to forcing functions — whereas we assume that state variables, actual or sensed, depend implicitly upon time. In other words the dependence of state variables upon time becomes explicit only when the dynamics equation (11) is solved for a particular trajectory.

The controller combines a feedforward (inverse model) and feedback (proportional derivative (PD)) component, representing the central neural command and the combined muscle and reflex impedance, respectively:

$$\begin{aligned} \mathbf{Q}(\mathbf{q}, \dot{\mathbf{q}}, \mathbf{q}_{\mathrm{d}}(t)) = {} & \mathbf{H}(\mathbf{q})\ddot{\mathbf{q}}_{\mathrm{d}}(t) + \mathbf{C}(\mathbf{q}, \dot{\mathbf{q}})\dot{\mathbf{q}} \\ & - \mathbf{K}_{\mathrm{p}}(\mathbf{q} - \mathbf{q}_{\mathrm{d}}(t)) - \mathbf{K}_{\mathrm{D}}(\dot{\mathbf{q}} - \dot{\mathbf{q}}_{\mathrm{d}}(t)), \end{aligned} \tag{14}$$

where $\mathbf{K}_{\mathrm{P}}$ and $\mathbf{K}_{\mathrm{D}}$ are proportional and derivative gains of the PD feedback controller, respectively, and we assume a perfect feedforward control model of inertial, Coriolis and centripetal forces (see Ref. [3] for detailed derivation). Note that the feedforward terms in this simulation assume a perfect model of the dynamic parameters **H** and **C**, based on the actual or sensed state variables. Alternative and more realistic models may postulate a dependence of **H** and **C** upon the desired states, and may include errors in the form of the inertial components and/or internal feedback delays.

After substituting (14) into (11) and defining an error term:

$$e(t) = q(t) - q_{\mathrm{d}}(t) \tag{15}$$

one obtains the following second-order error equation:

$$\mathbf{H}(\mathbf{q})\ddot{\mathbf{e}} + \mathbf{K}_{\mathrm{D}}\dot{\mathbf{e}} + \mathbf{K}_{\mathrm{P}}\mathbf{e} = 0, \tag{16}$$

and for positive gains the actual trajectory $\mathbf{q}(t)$ converges to the desired trajectory $\mathbf{q}_{\mathrm{d}}(t)$.

To simulate the interaction with a SLS we added an external force at the end-point of the arm, i.e., to the left side of (11):

$$\mathbf{H}(\mathbf{q})\ddot{\mathbf{q}} + \mathbf{C}(\mathbf{q}, \dot{\mathbf{q}})\dot{\mathbf{q}} + \mathbf{E}(\mathbf{q}|K, X_0) = \mathbf{Q}(\mathbf{q}, \dot{\mathbf{q}}, \mathbf{q}_{\mathrm{d}}(t)), \tag{17}$$

where according to (1) the SLS was implemented as:

$$\mathbf{E}(\mathbf{q}|K, X_0) = \begin{cases} \mathbf{J}_2^T(\mathbf{q})K(\boldsymbol{\alpha}(\mathbf{q}) - X_0) & \boldsymbol{\alpha}(\mathbf{q}) - X_0 > 0 \\ 0 & \boldsymbol{\alpha}(\mathbf{q}) - X_0 \leqslant 0, \end{cases} \tag{18}$$

and $\boldsymbol{\alpha}(\mathbf{q}) = x_2$ derived from the forward kinematics (7).

We assume perfect adaptation after each training phase, thus the controller includes a perfect internal representation of the disturbing force and we replace (14) with:

$$\begin{aligned} \mathbf{Q}(\mathbf{q}, \dot{\mathbf{q}}, \mathbf{q}_{\mathrm{d}}(t)) = {} & \mathbf{H}(\mathbf{q})\ddot{\mathbf{q}}_{\mathrm{d}}(t) + \mathbf{C}(\mathbf{q}, \dot{\mathbf{q}})\dot{\mathbf{q}} + \mathbf{E}(\mathbf{q}|K, X_0) \\ & - \mathbf{K}_{\mathrm{p}}(\mathbf{q} - \mathbf{q}_{\mathrm{d}}(t)) - \mathbf{K}_{\mathrm{D}}(\dot{\mathbf{q}} - \dot{\mathbf{q}}_{\mathrm{d}}(t)). \end{aligned} \tag{19}$$

Then, when the disturbing force is unexpectedly removed or the SLS's stiffness (K) is changed, an after effect will be observed due to the mismatch between the internal model and the actual external forces.

3.2. Simulations

3.2.1. Simulated Scenarios

With the arm model described above we simulated slicing movements into a SLS. We constructed the desired hand trajectory by concatenating two fifth-order polynomial representing two reaching movements to and from the target as derived by minimizing the jerk [40]:

$$x_{\mathrm{d}}(t) = \begin{cases} x_{\mathrm{s}} + (x_{\mathrm{s}} - x_{\mathrm{t}})\left(-6\left(\dfrac{2t}{\tau}\right)^5 + 15\left(\dfrac{2t}{\tau}\right)^4 - 10\left(\dfrac{2t}{\tau}\right)^3\right) \\ \quad 0 < t < \dfrac{\tau}{2} \\ x_{\mathrm{t}} + (x_{\mathrm{t}} - x_{\mathrm{s}}) \\ \times\left(-6\left(\dfrac{2t}{\tau} - 1\right)^5 + 15\left(\dfrac{2t}{\tau} - 1\right)^4 - 10\left(\dfrac{2t}{\tau} - 1\right)^3\right) \\ \quad \dfrac{\tau}{2} < t < \tau, \end{cases} \tag{20}$$

Table 2.
Arm model parameters (based on the literature [31, 32, 39])

Parameter	Shoulder	Forearm
Length (m)	$l_1 = 0.33$	$l_2 = 0.32$
Mass (kg)	$m_1 = 2.52$	$m_2 = 1.3$
Proportional gain (N/rad)	$K_{P1} = 20$	$K_{P2} = 20$
Derivative gain (Ns/rad)	$K_{D1} = 0.8$	$K_{D2} = 0.8$

where τ is the movement duration, and x_s and x_t are the start and target points, respectively.

We simulated the movement in catch trials following three different training conditions.

(i) Non-delayed SLS.

(ii) Delayed SLS (50 ms).

(iii) Boundary-shifted SLS (2 cm).

In all these conditions the surface stiffness during the training was $K = 375$ N/m. We assumed perfect learning and used an internal model equal to the trained surface in the simulations.

We simulated 10 catch trials in each condition using the experimental stiffness levels. In all these conditions the catch trials consisted of non-delayed non-shifted SLS.

The model parameters are summarized in Table 2. The center of mass and inertia parameters were calculated under the assumption of cylindrical links according to:

$$I = \frac{ml^2}{12}, \quad l_c = \frac{l}{2}. \tag{21}$$

3.2.2. Motormetric Curve Derivation

The motormetric curves are defined (Section 2.2.2) to address the stochastic nature of natural behavior. Since the arm model is deterministic the simulation results in each condition are either overshoot or undershoot. In order to derive predictions of motormetric curves based on the model one should add the sources of the natural noise to the simulation. Our simulation generates the exact distance from the target and not only a binary result of overshoot or undershoots. Therefore, we assume a monotonic relation between the amount of overshoot and the probability to overshoot in order to derive the motormetric curve.

The observed standard deviation of the error around the target in a typical subject was 1 cm, therefore neglecting the probability beyond 2 standard deviations we used the following relation between overshoot probability (P_{os}) and the simulated overshot in meters (os):

$$P_{os} = \begin{cases} 1 & os > 0.01 \\ 50(os + 0.01) & -0.01 \leqslant os \leqslant 0.01 \\ 0 & os < -0.01. \end{cases} \tag{22}$$

We simulated the overshoot probability for 10 levels of stiffness and fitted the motormetric curve as described for the psychometric curve (Section 2.2.1).

Following the arm dynamic model (16) we derived $p(K_{\text{trained}})$, the penetration (Section 2.2.2) in well-trained cases by solving the following dynamic equation:

$$\mathbf{D}(\mathbf{q}, \dot{\mathbf{q}}, \ddot{\mathbf{q}}) + \mathbf{E}_{\text{D}}(\mathbf{q}|K_{\text{trained}}) = \mathbf{Q}(\mathbf{q}, \dot{\mathbf{q}}, \mathbf{q}_{\text{d}}(t)) + \mathbf{E}_{\text{D}}(\mathbf{q}|K_{\text{trained}}), \tag{23}$$

where $\mathbf{D}(\mathbf{q}, \dot{\mathbf{q}}, \ddot{\mathbf{q}})$ is the arm dynamics, $\mathbf{E}_{\text{D}}(\mathbf{q}|K_{\text{trained}})$ is the SLS (boundary-shifted/delayed) perfectly represented by the controller and $\mathbf{Q}(\mathbf{q}, \dot{\mathbf{q}}, \mathbf{q}_{\text{d}}(t))$ is the control signal that corresponds to the control law specified at (14).

Then, for each catch trial with stiffness level K_{catch} we obtain $p(K_{\text{catch}})$ by solving the following dynamic equation:

$$\mathbf{D}(\mathbf{q}, \dot{\mathbf{q}}, \ddot{\mathbf{q}}) + \mathbf{E}(\mathbf{q}|K_{\text{catch}}) = \mathbf{Q}(\mathbf{q}, \dot{\mathbf{q}}, \mathbf{q}_{\text{d}}(t)) + \mathbf{E}_{\text{D}}(\mathbf{q}|K_{\text{trained}}) \tag{24}$$

i.e., we evaluate the change in state $\mathbf{q}$ due to altering from training SLS ($\mathbf{E}_{\text{D}}(\mathbf{q}|K_{\text{trained}})$) to the test SLS ($\mathbf{E}(\mathbf{q}|K_{\text{catch}})$).

The PMRE is defined as

$$\text{PMRE} = K_{\text{trained}} - K_{\text{catch}} \quad \text{s.t., } p(K_{\text{catch}}) = p(K_{\text{trained}}). \tag{25}$$

Since the absolute penetration equals the relative penetration in catch trials (as catch trials are neither delayed nor shifted), but differ in the training trials, the PMRE depends on the penetration coordinates (p_{a} or p_{r} as described in Section 2).

3.2.3. Simulated Results

In Fig. 6, we present the simulated motormetric curves of task *versus* baseline conditions, where the baseline is the first condition of the non-delayed non-shifted surface and the task is either the second condition (delayed surface) or the third condition (shifted surface).

First, we note that the amount of overshoot/undershoot at catch trials of the baseline condition is a monotonic function of the difference between the expected and the perturbing stiffness levels and the confidence interval around the PMRE includes the origin (Fig. 6, solid lines in all four planes). The simulation predicts positive PMRE for absolute penetration and negative PMRE for relative penetration in both conditions, i.e., for the D-surfaces.

4. Behavioral Results

4.1. Motormetric Curves of Delayed Stiffness and Boundary Shift

Figure 7 shows the measured motormetric curves for one of the subject. The PMRE for all subjects is depicted in Fig. 8.

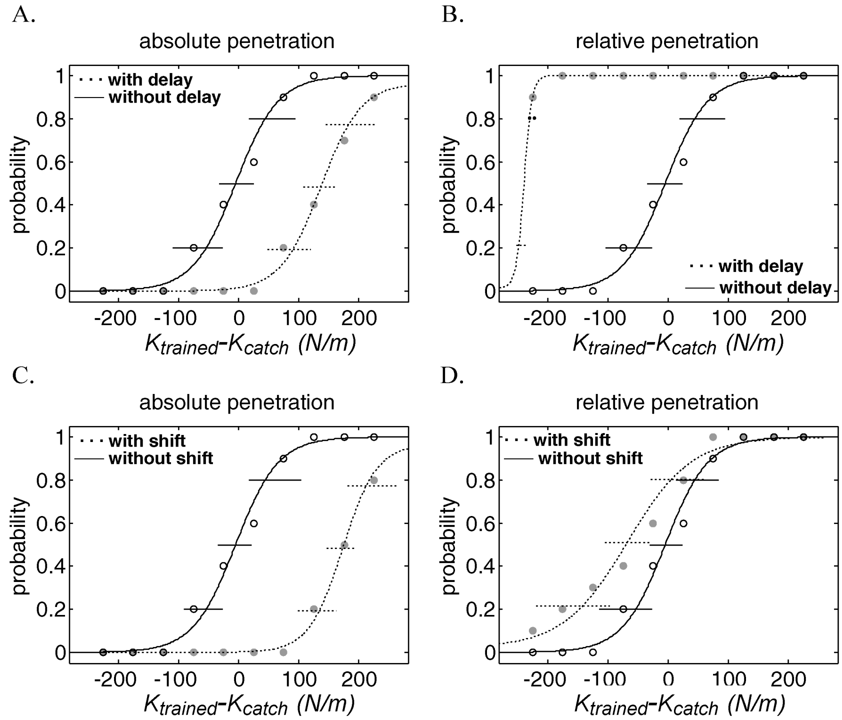

Figure 6. Simulated motormetric curves. The dots are the derived probability values based on the overshoot; the curve is the fitted motormetric curve and the horizontal lines indicating the 95% intervals for the fitted curve. The baseline condition of non-delayed non-shifted stiffness (solid) is depicted along with the delayed surface (A and B, dotted) or along with the shifted surface (C and D, dotted). Note that for both conditions (delayed and shifted surfaces) the simulated PMRE is positive for absolute penetration (A and C) and negative for relative penetration (B and D).

First, we note as predicted by the simulations that the amount of overshoot/undershoot at catch trials of the baseline condition is a monotonic function of the difference between the expected and the perturbing stiffness levels and the PMRE is close to zero (Fig. 7, solid lines in all four planes; Fig. 8, white bars).

As predicted by the simulations, the PMRE is positive for absolute penetration and negative for relative penetration in both experiments (Fig. 7, dotted line; Fig. 8 gray bars).

Figure 9 describes qualitatively the main result, where the dashed arrow represents the catch trial movement and the solid arrow represents the preceding trial. One can see that while the absolute penetration (the arrow head positions) undershoots the target, the relative penetration (dashed arrow) is longer for catch trials, showing relative overshoot. These results were completely predicted by the simulation described in the previous section. However, although the explicit representation of delay predicts the experimental results, so does the boundary-shift representation

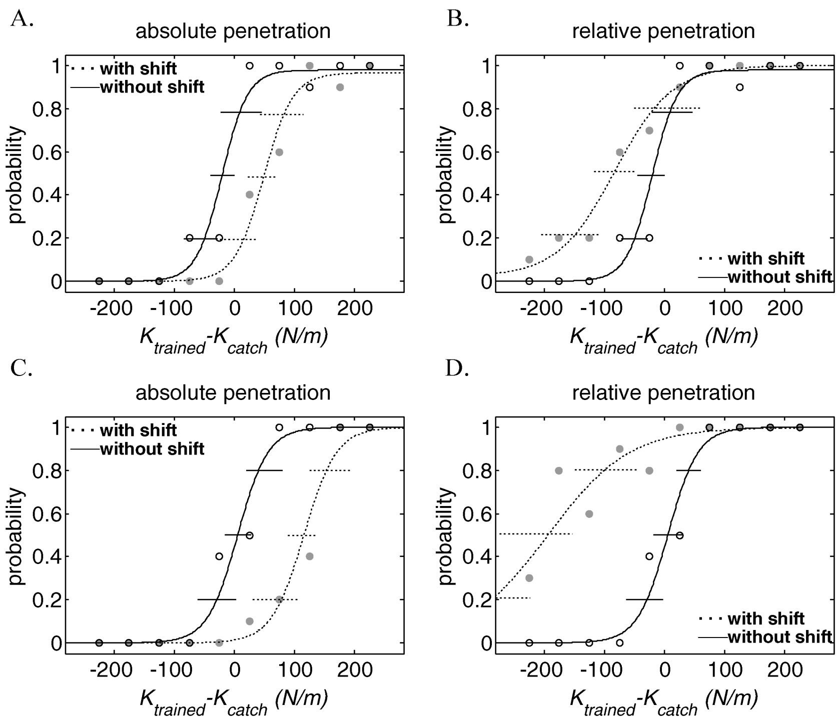

Figure 7. An example of a typical subject's motormetric curves from (A and B) delayed surface experiment and (C and D) boundary-shift experiment. The motormetric curves were derived using (A and C) absolute penetration and (B and D) relative penetration. The dots are the derived probability based on the measured overshoot; the curve is the fitted motormetric curve and the horizontal lines indicating the 95% intervals for the curve fitting.

and so would a representation of the delayed surface as a non-delayed surface with overestimated stiffness level.

4.2. Psychometric Curves of Boundary Shift

In Fig. 10, we present the psychometric curves for two typical subjects, one experienced boundary-shifted away (left) and the second experienced boundary-shifted towards him/her (right).

One can see that the shifted SLS is underestimated (positive PSE value) when shifted away from the subjects and overestimated (negative PSE value) when shifted towards the subject, in both cases the further surface is underestimated (Figs 10 and 11).

5. Discussion

We have reported some recent results obtained by applying a robotic paradigm to the study of haptic perception. In this study, the robotic device was used to simulate an altered virtual environment in which the delays between experienced forces and

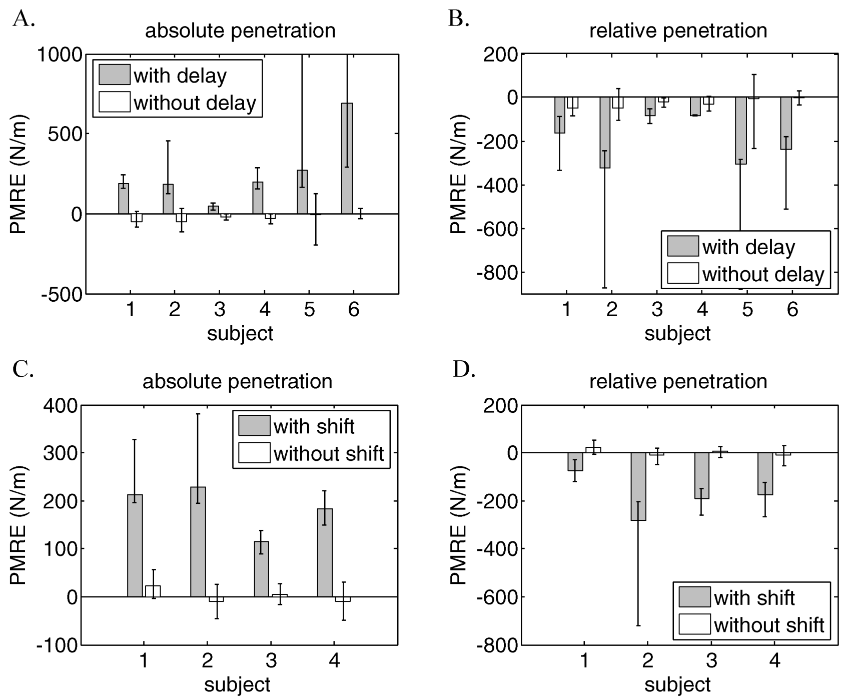

Figure 8. PMRE derived from motormetric curves fitted to all subjects' responses. (A and B) Delayed surface experiment ($n = 6$). (C and D) Boundary-shift experiment ($n = 4$). The bars show the fitted curve PMRE and the wings are the 95% confidence intervals for the fitted curve at the point of 50%.

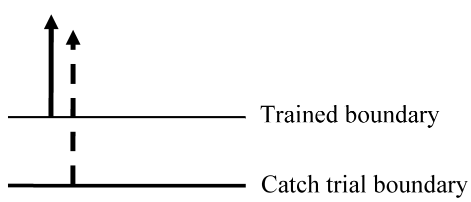

Figure 9. Schematic diagram of penetration in both experiments (boundary-shift and delayed stiffness for which the illustrated boundary represents the force encountering point). The dashed arrow represents the catch trial movement; the solid arrow represents preceding trial movement. The position of the arrow head represents the absolute penetration and its length represents the relative penetration. Note that the dashed arrow is longer than the solid arrow, indicating relative overshoot; however, the position of the dashed arrow head falls short of the solid arrow head, indicating absolute undershoot. This illustrates the simulation, as well as the measured results in both experiments, indicating absolute undershoot and relative overshoot.

displacements are manipulated together with the location of virtual surface boundaries. This allowed us to explore the perception of delayed, as well as shifted SLS by the human sensory-motor system. An arm model was simulated and motormetric curves were derived based on the overshoot of the simulated arm as well as the actual performance of the subjects. The simulated motor metric curves predicted

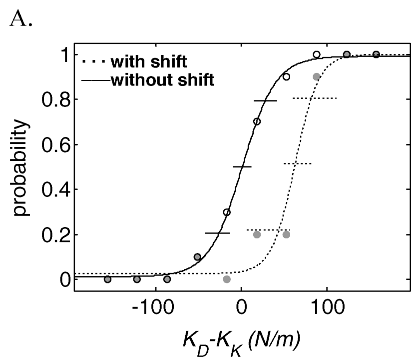

Figure 10. An example of psychometric curves for a typical subject. (A) SLS boundary-shifted away from the subject. The psychometric curve is shifted to the right, resulting in a positive PSE value, consistent with underestimation of the surface stiffness when the boundary is shifted away from the subject. (B) SLS boundary-shifted toward the subject. The psychometric curve is shifted to the left, resulting in a negative PSE value, consistent with overestimation of the surface stiffness when the boundary is shifted towards the subject. The dots are the ratios with which the subject answered that D is stiffer than K, the curve is the fitted psychometric curve, and the horizontal lines indicate the 95% intervals for the fitted curve.

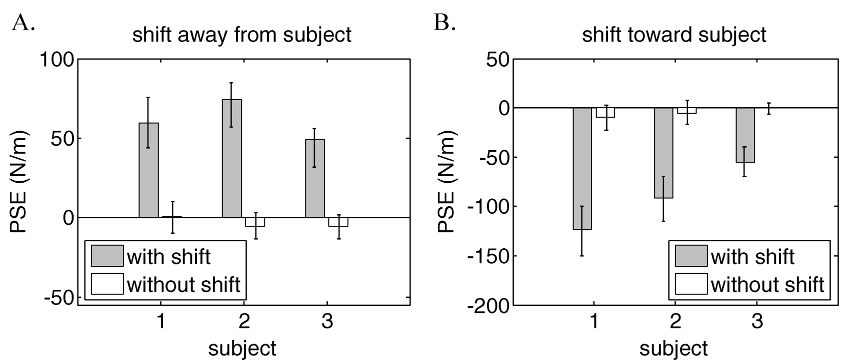

Figure 11. PSE derived from psychometric curves fitted to all subjects' responses. (A) SLS boundary-shifted away from the subject ($n = 3$), resulting in positive PSE values, i.e., underestimation of the shifted surface stiffness. (B) SLS boundary-shifted towards the subject ($n = 3$), resulting in negative PSE values, i.e., overestimation of the shifted surface stiffness. The bars show the fitted curve PSE and the wings are the 95% confidence intervals for the curve fit.

overestimation of the delayed stiffness as well as overestimation of the stiffness of the shifted surface. These predictions were clearly confirmed by the motormetric curves derived from the subjects' motor behavior. The psychometric curves based on the verbal response of subjects indicated overestimation of delayed stiffness (previous study), but underestimation of the stiffness in the case of shifted boundary.

The mismatch between the expected stiffness as measured by the motor behavior and the reported stiffness may indicate two parallel processes.

It was recently observed that reaching and grasping may be insensitive to illusions that dramatically influence the visual perception, suggesting that visual perception is mediated by neural processes that are functionally and anatomically distinct from those mediating the visual control of action [33–36].

This is not necessarily the case for our results, as there are a few assumptions that need to be tested before one can reach conclusive result as to the underlying brain mechanism. There were a few differences between the conditions of the adaptation experiment and those of the forced choice experiments, and it is also possible that the overshoot is not the proper measure to test the stiffness expectation.

Movement is the main output of the brain and therefore observing movement in a rich environment is a valuable tool to study the nervous system. Accurate haptic rendering by robotic devices is an essential tool to answer these open questions and unravel the neural mechanisms by which our brain forms effective representations of the environment in which we operate.

Acknowledgements

This research was supported by grant 2003021 from the United States–Israel Binational Science Foundation (BSF), Jerusalem, Israel, by the Davee Fund and by NINDS grant NS35673.

References

1. R. Shadmehr and S. P. Wise, *The Computational Neurobiology of Reaching and Pointing: A Foundation for Motor Learning*. MIT Press, Cambridge, MA (2005).
2. K. A. Thoroughman and R. Shadmehr, Learning of action through adaptive combination of motor primitives [see comments], *Nature* **407**, 742–747 (2000).
3. R. Shadmehr and F. A. Mussa-Ivaldi, Adaptive representation of dynamics during learning of a motor task, *J. Neurosci.* **14**, 3208–3224 (1994).
4. R. A. Scheidt, J. B. Dingwell and F. A. Mussa-Ivaldi, Learning to move amid uncertainty, *J. Neurophysiol.* **86**, 971–985 (2001).
5. A. Karniel and F. A. Mussa-Ivaldi, Sequence, time, or state representation: how does the motor control system adapt to variable environments?, *Biol. Cybernet.* **89**, 10–21 (2003).
6. H. Gomi and M. Kawato, Equilibrium-point control hypothesis examined by measured arm stiffness during multijoint movement, *Science* **272**, 117–120 (1996).
7. M. A. Smith, A. Ghazizadeh and R. Shadmehr, Interacting adaptive processes with different timescales underlie short-term motor learning, *PloS Biol.* **4**, 1035–1043 (2006).
8. V. S. Chib, J. L. Patton, K. M. Lynch and F. A. Mussa-Ivaldi, Haptic identification of surfaces as fields of force, *J. Neurophysiol.* **95**, 1068–1077 (2006).
9. M. A. Smith, J. Brandt and R. Shadmehr, Motor disorder in Huntington's disease begins as a dysfunction in error feedback control, *Nature* **403**, 544–549 (2000).
10. J. L. Patton, M. E. Stoykov, M. Kovic and F. A. Mussa-Ivaldi, Evaluation of robotic training forces that either enhance or reduce error in chronic hemiparetic stroke survivors, *Exp. Brain Res.* **168**, 368–383 (2006).
11. H. I. Krebs, N. Hogan, M. L. Aisen and B. T. Volpe, Robot-aided neurorehabilitation, *IEEE Trans. Rehabil. Eng.* **6**, 75–87 (1998).

12. H. I. Krebs, N. Hogan, W. Hening, S. V. Adamovich and H. Poizner, Procedural motor learning in Parkinson's disease, *Exp. Brain Res.* **141**, 425–437 (2001).
13. J. Biggs and M. A. Srinivasan, Haptic interfaces, in: *Handbook of Virtual Environments* (K. Stanney, Ed.), pp. 93–115. Lawrence Earlbaum, London (2002).
14. M. O. Ernst, M. S. Banks and H. H. Bulthoff, Touch can change visual slant perception, *Nat. Neurosci.* **3**, 69–73 (2000).
15. M. O. Ernst and M. S. Banks, Humans integrate visual and haptic information in a statistically optimal fashion, *Nature* **415**, 429–433 (2002).
16. E. D. Fasse, N. Hogan, B. A. Kay and F. A. Mussa-Ivaldi, Haptic interaction with virtual objects — Spatial perception and motor control, *Biol. Cybernet.* **82**, 69–83 (2000).
17. I. M. L. C. Vogels, Detection of temporal delays in visual–haptic interfaces, *Hum. Factors* **46**, 118–134 (2004).
18. G. Niemeyer and J. J. E. Slotine, Telemanipulation with time delays, *Int. J. Robotics Res.* **23**, 873–890 (2004).
19. B. Hannaford, A design framework for teleoperators with kinesthetic feedback, *IEEE Trans. Robotics Automat.* **5**, 426–434 (1989).
20. R. J. Anderson and M. W. Spong, Bilateral control of teleoperators with time-delay, *IEEE Trans. Automatic Control* **34**, 494–501 (1989).
21. R. J. Anderson and M. W. Spong, Asymptotic stability for force reflecting teleoperators with time-delay, *Int. J. Robotics Res.* **11**, 135–149 (1992).
22. R. C. Miall, D. J. Weir, D. M. Wolpert and J. F. Stein, Is the cerebellum a Smith Predictor?, *J. Motor Behav.* **25**, 203–216 (1993).
23. R. C. Miall and J. K. Jackson, Adaptation to visual feedback delays in manual tracking: evidence atainst the Smith Predictor model of human visually guided action, *Exp. Brain Res.* **172**, 77–84 (2006).
24. S. G. Massaquoi and J. J. E. Slotine, The intermediate cerebellum may function as wave-variable processor, *Neurosci. Lett.* **215**, 60–64 (1996).
25. J. R. Lackner and P. DiZio, Rapid adaptation to Coriolis force perturbations of arm trajectories, *J. Neurophysiol.* **72**, 299–313 (1994).
26. T. Flash and I. Gurevich, Models of motor adaptation and impedance control in human arm movements, in: *Self-Organization, Computational Maps, and Motor Control* (P. Morasso and V. Sanguineti, Eds), Amsterdam: Elsevier Science (1997), pp. 423–481.
27. M. A. Conditt and F. A. Mussa-Ivaldi, Central representation of time during motor learning, *Proc. Nat. Acad. Sci. USA* **96**, 11625–11630 (1999).
28. A. Pressman, A. Karniel and F. A. Mussa-Ivaldi, Perception of delayed stiffness, presented at: *Biorob2006*, Pisa (2006).
29. F. A. Wichmann and N. J. Hill, The psychometric function: II. Bootstrap-based confidence intervals and sampling, *Percept. Psychophys.* **63**, 1314–1329 (2001).
30. F. A. Wichmann and N. J. Hill, The psychometric function: I. Fitting, sampling, and goodness of fit, *Percept. Psychophys.* **63**, 1293–1313 (2001).
31. F. A. Mussa-Ivaldi, N. Hogan and E. Bizzi, Neural, mechanical, and geometric factors subserving arm posture in humans, *J. Neurosci.* **5**, 2732–2743 (1985).
32. A. Karniel and G. F. Inbar, A model for learning human reaching movements, *Biol. Cybernet.* **77**, 173–183 (1997).
33. D. P. Carey, Do action systems resist visual illusions?, *Trends Cognit. Sci.* **5**, 109–113 (2001).
34. T. Ganel and M. A. Goodale, Visual control of action but not perception requires analytical processing of object shape, *Nature* **426**, 664–667 (2003).

35. Y. Hu and M. A. Goodale, Grasping after delay shifts size scaling from absolute to relative metrics, *J. Cognit. Neurosci.* **12**, 856–868 (2000).
36. M. A. Goodale and A. D. Milner, Seperate visoual pathways for perception and action, *Trends Neurosci.* **15**, 20–25 (1992).
37. A. J. M. Foulkes and R. C. Miall, Adaptation to visual feedback delays in a human manual tracking task, *Exp. Brain Res.* **131**, 101–110 (2000).
38. D. W. Cunningham, A. Chatziastros, M. von der Heyde and H. H. Bulthoff, Driving in the future: Temporal visoumotor adaptation and generalization, *J. Vis.* **1**, 88–98 (2001).
39. H. Gomi and R. Osu, Task-dependent viscoelasticity of human multijoint arm and its spatial characteristics for interaction with environments, *J. Neurosci.* **18**, 8965–8978 (1998).
40. T. Flash and N. Hogan, The coordination of arm movements: an experimentally confirmed mathematical model, *J. Neurosci.* **5**, 1688–1703 (1985).

About the Authors

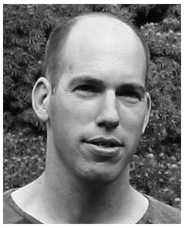

Assaf Pressman received his BS degree in 1998 and his MS degree in 2001 in Electrical Engineering from Ben-Gurion University of the Negev, Israel. During his undergraduate studies he worked for Applied Materials Corp., Rehovot, Israel. From 2000 to 2002, he worked in Widemed (Omer, Israel) developing algorithms for automatic sleep apnea identification. From 2002 to 2004, he worked as a System Engineer and Algorithm Developer in the Israel Aircraft industry (Ashdod, Israel). Since 2004, he has been in the Robotics laboratory at the Sensory Motor Performance Program, Rehabilitation Institute of Chicago, Chicago, IL, USA. Currently, he is enrolled in the PhD program in the Department of Biomedical Engineering at Ben-Gurion University of the Negev, under the supervision of Dr Amir Karniel. His research interests include brain theory, biomedical signal processing, motor control and motor learning.

Ilana Nisky received her BS degree (Summa Cum Laude) from the Department of Biomedical Engineering, Ben-Gurion University of the Negev, Israel, in 2006, and currently is studying towards a PhD (direct track) in Biomedical Engineering. She received the Wolf Foundation scholarship for undergraduate students and currently is a Kreitman Foundation Fellow. Her research interests include motor control, robotics, human and machine learning, teleoperation and human–machine interfaces.

Amir Karniel received the BS degree (Cum Laude) in 1993, the MS degree in 1996 and the PhD degree in 2000, all in Electrical Engineering, from the Technion—Israel Institute of Technology, Haifa, Israel. He served 4 years in the Israeli Navy as an Electronics Technician and worked during his undergraduate studies at Intel Corp., Haifa, Israel. He received the E. I. Jury award for excellent students in the area of systems theory and the Wolf Scholarship award for excellent research students. For 2 years he had been a Post-Doctoral Fellow at the Department of Physiology, Northwestern University Medical School and the Robotics Lab of the Rehabilitation Institute of Chicago, Chicago, IL, USA. Since 2003, he has been with the Department of Biomedical Engineering at Ben-Gurion University (BGU) of the Negev where he serves as the Head of the Teaching Committee, Head of the Computational Motor Control Laboratory and Organizer of the Annual International Computational Motor Control Workshop. During the last 3 years he won a Young Scientist BSF grant, was promoted to Senior Lecturer at the BGU and to

Senior Member of the IEEE, and obtained a grant from the National Institute of Psychobiology in Israel. His research interests include brain theory, neural networks, motor control and motor learning.

Ferdinando A. Mussa-Ivaldi is a member of the IEEE. He has a degree (Laurea) in Physics from the University of Torino (1978) and a PhD in Biomedical Engineering from the Politecnico of Milano (1987). He is Professor of Physiology, Physical Medicine and Rehabilitation and Biomedical Engineering at Northwestern University, Chicago, IL, USA. He is a Senior Research Scientist at the Rehabilitation Institute of Chicago, where he founded and directs the Robotics Laboratory. His areas of interest and expertise include robotics, neurobiology of the sensory-motor system and computational neuroscience. Among his achievements are the first measurement of human arm multi-joint impedance, the development of a technique for investigating the mechanisms of motor learning through the application of deterministic force fields, the discovery of a family of integrable generalized inverses for redundant kinematic chains, the discovery of functional modules within the spinal cord that generate a discrete family of force fields, the development of a theoretical framework for the representation, generation and learning of limb movements, and the development of the first neurorobotic system in which the brainstem of a lamprey controls the behavior of a mobile robot through a closed-loop interaction. He has 110 full-length publications and 85 abstracts. He is on the Editorial Board of the *Journal of Neural Engineering* and *Journal of Motor Behavior*, and is a Member of the Society for Neuroscience and the Society for the Neural Control of Movement.